Tensor-based High-Accuracy Position Estimation for 5G mmWave Massive MIMO Systems

Zhipeng Lin[†*], Tiejun Lv[†], J. Andrew Zhang[*], and Ren Ping Liu[*]
[†]School of Information and Communication Engineering
Beijing University of Posts and Telecommunications, Beijing, China
[*]School of Electrical and Data Engineering, University of Technology Sydney, Sydney, Australia
Email: {linlzp, lvtiejun}@bupt.edu.cn, {Andrew.Zhang, RenPing.Liu}@uts.edu.au

***Abstract*—Highly accurate localization is important for wireless communications. In this paper, we propose a new tensor-based positioning method for 5G wideband mmWave massive MIMO systems. We first develop an extended multidimensional interpolation (E-MI)-based method as the preprocessing step to suppress the frequency-dependence of the array steering vectors. By using this method, the data across the whole frequency band can be processed jointly, and the high temporal resolution offered by wideband mmWave signals can be exploited. Then, we propose a parameter decoupling (PD)-based tensor multiparameter estimation algorithm. This algorithm can suppress the noises in all of temporal, spatial and frequency domains, and thus all the parameters can be precisely estimated. A simplified perturbation term (S-PT)-based method is also presented to match the estimated parameters at low complexity. Based on the quasi-optical property of mmWave signals, we propose a novel method to compute the 3D coordinates of the target. Simulation results demonstrate the effectiveness of the proposed positioning method in the end.**

***Index Terms*—Wideband mmWave, massive MIMO, tensor, multidimensional interpolation, multiparameter matching**

I. Introduction

Accurate localization in Global Position System (GPS)-denied environments is becoming increasingly important for rapidly growing location-based applications [1]. Combining with high-directivity massive multiple-input multiple-output (MIMO) techniques, large-bandwidth millimeter-wave (mmWave) systems are promising for achieving precise localization thanks to its potentially high temporal resolution [2]. However, most of the current positioning algorithms proposed for mmWave massive MIMO systems, such as [1], [3], are based on the assumption that the line-of-sight (LOS) path exists between mobile station (MS) and base station (BS), and they only consider up to two-dimensional (2D) scenarios, which could be limited in practice.

To achieve 3D localization, the azimuth and elevation angles of arrival/departure (AOAs/AODs) of each path, as well as the propagation delay, need to be estimated. However, traditional multiparameter estimation is typically matrix-based. When using these methods, the received multidimensional data needs to be stacked and processed in the two-dimensional space-time matrix, and thus the relations between each dimension/domain (e.g., space, time, and frequency) of the received data would be damaged [4]. In addition, these parameters (e.g., AOA, AOD, and delay) are coupled in the space-time matrix. Therefore, before using subspace-based algorithms, such as multiple signal classification (MUSIC) and estimation of signal parameters via rotational invariance technique (ESPRIT) [2], the space-time matrix has to be divided into multiple (≥ 6) subarrays to decouple them, increasing the estimation complexity.

Specific to mmWave massive MIMO systems, another problem is that the variation of channel parameters across frequencies can be non-trivial due to the large bandwidth. This issue has been typically ignored in the previous studies. One existing solution, i.e., incoherent signal-subspace processing (ISSP) [5], divides the wide frequency band into non-overlapping narrowbands. By assuming that the channel remains constant in each narrowband, positioning algorithms are applied to each narrowband separately, and thus extra processing steps are needed to combine the results from individual narrowbands. As a result, the quantity of computation will be increased.

In this paper, we propose a new 3D positioning method for wideband mmWave massive MIMO systems. An extended multidimensional interpolation (E-MI) preprocessing step is first introduced to jointly process the data across the whole frequency band. We then propose a parameter decoupling (PD)-based tensor multiparameter estimation algorithm, which works for beyond LOS (BLOS) scenarios, where both LOS and non-LOS paths may exist. By using this method, the space-time matrix only needs to be divided into three subarrays for multiparameter decoupling, and the data received from almost all the antennas can be used for parameter estimation. In addition, the proposed algorithm also formulates and processes the data in the tensor form. Thus, the intrinsic multidimensional features of the received data can be fully exploited, and the noises in all the domains (i.e., space, time, and frequency) can be suppressed separately. Considering that the estimated parameters of each path cannot be matched automatically, a simplified perturbation term (S-PT)-based multiparameter matching method is presented, and the process of computing the coordinates of the target is also discussed in the end. The simulation results demonstrate that our proposed method can achieve highly accurate localization.

Preliminary: The tensor operations used this paper are

The financial support of the National Natural Science Foundation of China (NSFC) (Grant No. 61671072) is gratefully acknowledged.

consistent with [6]. $\mathcal{A} \in \mathbb{C}^{I_1 \times I_2 \times \cdots \times I_N}$ represents an order-N tensor, whose elements (entries) are $a_{i_1,i_2,\cdots,i_N}$, $i_n = 1, 2, \ldots, I_n$; $\mathbf{A}_{(n)} \in \mathbb{C}^{I_n \times (I_1 I_2 \cdots I_N / I_n)}$ denotes the mode-n unfolding (also known as matricization) of $\mathcal{A}$; $\circ$ and $\times_n$ are the tensor outer product and n-mode product.

In this paper, we also use the higher-order singular value decomposition (HOSVD), which is given by

$$\mathcal{A} = \mathcal{S} \times_1 \mathbf{U}^{(1)} \times_2 \mathbf{U}^{(2)} \cdots \times_N \mathbf{U}^{(N)}, \tag{1}$$

where the core tensor $\mathcal{S} \in \mathbb{C}^{I_1 \times I_2 \times \cdots \times I_N}$ is all-orthogonal and in descending order [6], and $\mathbf{U}^{(n)} \in \mathbb{C}^{I_n \times I_n}$ is the unitary left singular matrix of $\mathbf{A}_{(n)}$ $(n = 1, 2, \ldots, N)$.

II. System Model

We consider a 3D positioning problem, where a BS at a known position localizes an MS by using the received signals from the MS. We consider a wideband mmWave orthogonal frequency division multiplexing (OFDM) system with N_{T} transmit and N_{R} receive antennas. The received baseband signal at subcarrier $n = 1, 2, \ldots, N$, can be represented as

$$\mathbf{y}[n] = \mathbf{H}[n]\mathbf{x}[n] + \mathbf{w}[n], \tag{2}$$

where $\mathbf{x}[n] \in \mathbb{C}^{N_{\mathrm{T}} \times 1}$, $\mathbf{H}[n] \in \mathbb{C}^{N_{\mathrm{R}} \times N_{\mathrm{T}}}$, and $\mathbf{w}[n] \in \mathbb{C}^{N_{\mathrm{R}} \times 1}$ represent the transmitted signal vector, the channel matrix, and the Gaussian noise at subcarrier n, respectively. In this paper, we assume that the transmitted signal, $\mathbf{x}[n]$, is known, and there are in total N_{p} BLOS paths. $\mathbf{H}[n]$ can be mathematically expressed as

$$\mathbf{H}[n] = \mathbf{A}_{\mathrm{R}}[n]\Lambda[n]\mathbf{A}_{\mathrm{T}}^{H}[n] + \mathbf{N}[n], \tag{3}$$

where $[\mathbf{A}_{\mathrm{R}}[n]]_{:,l} = \mathbf{a}_{\mathrm{R},n}(\phi_{\mathrm{R},l}, \theta_{\mathrm{R},l})$ and $[\mathbf{A}_{\mathrm{T}}[n]]_{:,l} = \mathbf{a}_{\mathrm{T},n}(\phi_{\mathrm{T},l}, \theta_{\mathrm{T},l})$ are the array steering matrices of the receive antenna, respectively, with $\theta_{\mathrm{R},l}/\phi_{\mathrm{R},l}$ and $\theta_{\mathrm{T},l}/\phi_{\mathrm{T},l}$ being the azimuth/elevation of AOAs and AODs of the l-th path; $\mathbf{N}[n]$ is the white-Gaussian noise. $\Lambda[n]$=diag$\{\beta_1 e^{-j2\pi f_n \tau_1}, \ldots, \beta_{N_{\mathrm{p}}} e^{-j2\pi f_n \tau_{N_{\mathrm{p}}}}\}$, where τ_l and β_l denote the delay and the complex amplitude of the l-th path signal, respectively, and N_{p} represents the total number of paths. $f_n = f_0 + (n-1)\Delta_{\mathrm{F}}$ is the frequency at the n-th subcarrier, where f_0 is the carrier frequency at the lower end of the band and Δ_{F} is the subcarrier spacing. Consider that a large uniform rectangular array (URA) is used at both BS and MS. Therefore, the receive array steering vector can be constructed as

$$\mathbf{a}_{\mathrm{R},n}(\phi_{\mathrm{R},l}, \theta_{\mathrm{R},l}) = \mathbf{a}_{\mathrm{RX},n}(\phi_{\mathrm{R},l}, \theta_{\mathrm{R},l}) \otimes \mathbf{a}_{\mathrm{RY},n}(\phi_{\mathrm{R},l}, \theta_{\mathrm{R},l}), \tag{4}$$

where $\otimes$ denotes the Kronecker product,

$$[\mathbf{a}_{\mathrm{RX},n}(\phi_{\mathrm{R},l}, \theta_{\mathrm{R},l})]_{n_{\mathrm{RX}},1} = \frac{1}{\sqrt{N_{\mathrm{RX}}}} \exp(j\frac{2\pi f_n}{c} d_{\mathrm{R}}(n_{\mathrm{RX}} - 1)\sin(\phi_{\mathrm{R},l})\cos(\theta_{\mathrm{R},l}))$$

and

$$[\mathbf{a}_{\mathrm{RY},n}(\phi_{\mathrm{R},l}, \theta_{\mathrm{R},l})]_{n_{\mathrm{RY}},1} = \frac{1}{\sqrt{N_{\mathrm{RY}}}} \exp(j\frac{2\pi f_n}{c} d_{\mathrm{R}}(n_{\mathrm{RY}} - 1)\sin(\phi_{\mathrm{R},l})\sin(\theta_{\mathrm{R},l}))$$

are array response vectors along the x- and y-directions, respectively, and c denotes the speed of light. In the above equations, N_{RX} and N_{RY} represent the number of antennas deployed along the x- and y-directions, so $N_{\mathrm{R}} = N_{\mathrm{RY}} N_{\mathrm{RY}}$; and d_{R} denotes the distance between two adjacent antennas. The transmit array steering vector, $\mathbf{a}_{\mathrm{T},n}(\phi_{\mathrm{T},l}, \theta_{\mathrm{T},l})$, is defined in the same way.

III. Extended Multidimensional Interpolation (E-MI)

In this section, an E-MI-based method is developed based on the spatial interpolation [7], to map the frequency-dependent array steering vectors at each subcarrier frequency, f_n, to the reference frequency f_0. As a result, the frequency-dependence of array steering vectors is suppressed, and the information in all frequency bands can be processed jointly in the subsequent parameter estimation (as described in Section IV).

Define virtual antenna spacing, $d_{\mathrm{R}}[n] = f_0 d_{\mathrm{R}}/f_n$ and $d_{\mathrm{T}}[n] = f_0 d_{\mathrm{T}}/f_n$, as the sampling intervals, then the virtual array steering vectors can be calculated as$[\tilde{\mathbf{a}}_{\mathrm{R},n}(\phi_{\mathrm{R},l}, \theta_{\mathrm{R},l})]_{n_{\mathrm{R}},1} = [\mathbf{a}_{\mathrm{R},0}(\phi_{\mathrm{R},l}, \theta_{\mathrm{R},l})]_{n_{\mathrm{R}},1}$ and $[\tilde{\mathbf{a}}_{\mathrm{T},n}(\phi_{\mathrm{R},l}, \theta_{\mathrm{R},l})]_{n_{\mathrm{T}},1} = [\mathbf{a}_{\mathrm{T},0}(\phi_{\mathrm{R},l}, \theta_{\mathrm{R},l})]_{n_{\mathrm{T}},1}$. Thus, the channel matrix can be formulated as

$$\tilde{\mathbf{H}}[n] = \mathbf{A}_{\mathrm{R}}[0]\Lambda[n]\mathbf{A}_{\mathrm{T}}^{H}[0] + \tilde{\mathbf{N}}[n], \tag{5}$$

where the array steering matrices become constants for all frequencies. For convenience, in the following sections, we use $\mathbf{A}_{\mathrm{R}}$ and $\mathbf{A}_{\mathrm{T}}$ to represent $\mathbf{A}_{\mathrm{R}}[0]$ and $\mathbf{A}_{\mathrm{T}}[0]$, respectively.

However, in practice, it is difficult to realize perfect resampling by the Shannon-Whittaker interpolation [8], so in this paper we propose an alternative approximation method, E-MI, for channel matrix reconstruction. More precisely, by applying the proposed extended multidimensional interpolation to (3), we have

$$\left[\tilde{\mathbf{H}}_{\mathrm{A}}[n]\right]_{n_{\mathrm{R}},n_{\mathrm{T}}} = [\mathbf{H}[n]]_{n_{\mathrm{R}},n_{\mathrm{T}}} + \frac{d_{\mathrm{R}}[n]}{d_{\mathrm{R}}}(\Delta_{\mathbf{H}_{\mathrm{RY}}} + \Delta_{\mathbf{H}_{\mathrm{RX}}}) + \frac{d_{\mathrm{T}}[n]}{d_{\mathrm{T}}}(\Delta_{\mathbf{H}_{\mathrm{TY}}} + \Delta_{\mathbf{H}_{\mathrm{TX}}}), \tag{6}$$

where

$$\Delta_{\mathbf{H}_{\mathrm{RY}}} = [\mathbf{H}[n]]_{(n_{\mathrm{R}}+1),n_{\mathrm{T}}} - [\mathbf{H}[n]]_{n_{\mathrm{R}},n_{\mathrm{T}}}, \tag{7}$$

$$\Delta_{\mathbf{H}_{\mathrm{RX}}} = [\mathbf{H}[n]]_{(n_{\mathrm{R}}+N_{\mathrm{RH}}),n_{\mathrm{T}}} - [\mathbf{H}[n]]_{n_{\mathrm{R}},n_{\mathrm{T}}}, \tag{8}$$

$$n_{\mathrm{R}} = N_{\mathrm{RY}}(n_{\mathrm{RX}} - 1) + n_{\mathrm{RY}}, \tag{9}$$

$$n_{\mathrm{T}} = N_{\mathrm{TY}}(n_{\mathrm{TX}} - 1) + n_{\mathrm{TY}}. \tag{10}$$

The terms $\Delta_{\mathbf{H}_{\mathrm{TY}}}$ and $\Delta_{\mathbf{H}_{\mathrm{TX}}}$ can be calculated similarly.

After the E-MI preprocessing, the resultant array steering vectors do not vary with the frequency, and thus the data in all frequency bands can be processed jointly. As a result, the high temporal resolution offered by the large bandwidth of mmWave signal can be exploited for target localization.

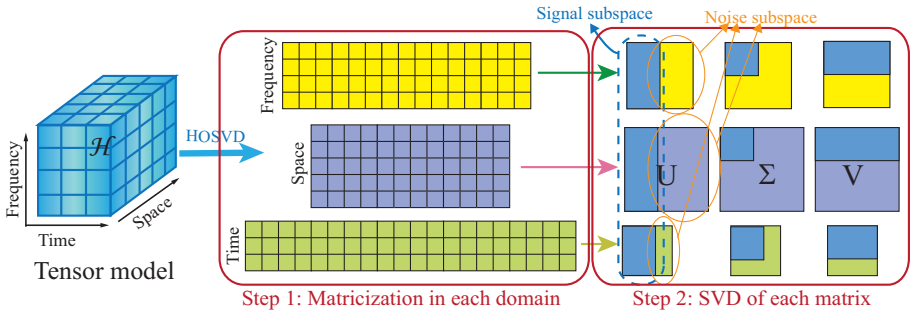

Fig. 1. Illustration of the HOSVD of channel tensor model.

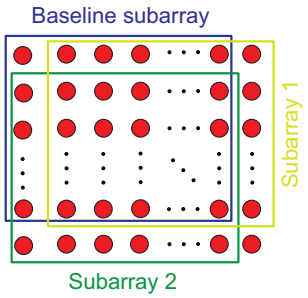

Fig. 2. Illustration of the subarray division.

IV. 3D Localization

In this section, we propose a novel PD-based tensor multi-parameter estimation algorithm to estimate the angle and delay of each path. An S-PT-based method is then proposed to match the estimated parameter pairs. We also introduce the method of computing the 3D coordinates of the target based on the estimated multiple channel parameters.

A. Truncated HOSVD Model

To process the signals in all frequency bands simultaneously, we collect the data at all frequencies and express the channel matrix in (6) in the tensor form. After E-MI processing, the element of (6) associated with the n-th subcarrier at the m-th time frame $(m = 1, \ldots, M)$ can be expressed as

$$h_{n_{\mathrm{R}},n_{\mathrm{T}},n,m} = \sum_{l=1}^{N_{\mathrm{p}}} \beta_{l,m} a_{\mathrm{R},n_{\mathrm{R}}}(\phi_{\mathrm{R},l},\theta_{\mathrm{R},l}) \times a_{\mathrm{T},n_{\mathrm{T}}}(\phi_{\mathrm{T},l},\theta_{\mathrm{T},l}) a_{\mathrm{F},n}(\tau_l) + n_{n_{\mathrm{R}},n_{\mathrm{T}},n,m}, \quad (11)$$

where $a_{\mathrm{F},n}(\tau_l) = e^{-j2\pi f_n \tau_l}$, and $n_{n_{\mathrm{R}},n_{\mathrm{T}},n,m}$ denotes the additive noise component. (11) can be be expressed concisely as

$$\mathcal{H} = \mathcal{A} \times_4 \mathbf{B} + \mathcal{N}, \quad (12)$$

where $[\mathbf{B}]_{m,l} = \beta_{l,m}$ and $\mathcal{N}$ collects all the noise samples. In (12), $\mathcal{A}$ is constructed by concatenating the N_{p} array response tensors $\mathcal{A}_l$, which can be expressed as

$$\mathcal{A}_l = \mathbf{a}_{\mathrm{R}}(\phi_{\mathrm{R},l},\theta_{\mathrm{R},l}) \circ \mathbf{a}_{\mathrm{T}}(\phi_{\mathrm{T},l},\theta_{\mathrm{T},l}) \circ \mathbf{a}_{\mathrm{F}}(\tau_l), \quad (13)$$

where $[\mathbf{a}_{\mathrm{F}}(\tau_l)]_{n,1} = a_{\mathrm{F},n}(\tau_l)$. According to the CANDECOMP/PARAFAC (CP) decomposition [6], by substituting (13) into (12), we can obtain

$$\mathcal{H} = \mathcal{L} \times_1 \mathbf{A}_{\mathrm{R}} \times_2 \mathbf{A}_{\mathrm{T}} \times_3 \mathbf{A}_{\mathrm{F}} \times_4 \mathbf{B} + \mathcal{N} \quad (14)$$

where $[\mathbf{A}_{\mathrm{F}}]_{:,l} = \mathbf{a}_{\mathrm{F}}(\tau_l)$ and $\mathcal{L} \in \mathbb{C}^{N_{\mathrm{p}} \times N_{\mathrm{p}} \times N_{\mathrm{p}} \times N_{\mathrm{p}}}$ is an identity superdiagonal tensor.

Given the typically sparse multipath propagation of mmWave, the number of the received paths is typically much smaller than those of the antennas, subcarriers, and time frames, i.e., $N_{\mathrm{p}} \ll \min(N_{\mathrm{R}}, N_{\mathrm{T}}, N, M)$. Thus, we can construct a low-rank truncated HOSVD model of the noise-free $\mathcal{H}$ [6] to suppress the received noise components in each domain (space, frequency, and time).

We first use HOSVD to conduct the SVD model of $\mathcal{H}$ in each dimension. The HOSVD of $\mathcal{H}$ is given by

$$\mathcal{H} = \mathcal{S} \times_1 \mathbf{U}_{\mathrm{R}} \times_2 \mathbf{U}_{\mathrm{T}} \times_3 \mathbf{U}_{\mathrm{F}} \times_4 \mathbf{U}_{\mathrm{TM}}, \quad (15)$$

where the unitary matrices, $\mathbf{U}_{\mathrm{R}}$, $\mathbf{U}_{\mathrm{T}}$, $\mathbf{U}_{\mathrm{F}}$, and $\mathbf{U}_{\mathrm{TM}}$, are the left singular matrices of the unfolding of tensor $\mathcal{H}$ in each mode, and the core tensor $S \in \mathbb{C}^{N_{\mathrm{R}} \times N_{\mathrm{T}} \times N \times M}$ is obtained by

$$\mathcal{S} = \mathcal{H} \times_1 \mathbf{U}_{\mathrm{R}}^H \times_2 \mathbf{U}_{\mathrm{T}}^H \times_3 \mathbf{U}_{\mathrm{F}}^H \times_4 \mathbf{U}_{\mathrm{TM}}^H. \quad (16)$$

Because the ranks of $\mathcal{H}$ in all the domains are N_{p}, the SVD of the mode-1 unfolding $\mathbf{H}_{(1)}$ (corresponding the space domain of receive antenna) can be written as

$$\mathbf{H}_{(1)} = \mathbf{U}_{\mathrm{R}} \mathbf{\Sigma}_{\mathrm{R}} \mathbf{V}_{\mathrm{R}}^H = [\mathbf{U}_{\mathrm{R,s}}\ \mathbf{U}_{\mathrm{R,n}}] \times \begin{bmatrix} \mathbf{\Sigma}_{\mathrm{R,s}} & \mathbf{0}_{N_{\mathrm{p}} \times (N_{\mathrm{T}} N M - N_{\mathrm{p}})} \\ \mathbf{0}_{(N_{\mathrm{R}} - N_{\mathrm{p}}) \times N_{\mathrm{p}}} & \mathbf{\Sigma}_{\mathrm{R,n}} \end{bmatrix} [\mathbf{V}_{\mathrm{R,s}}\ \mathbf{V}_{\mathrm{R,n}}]^H, \quad (17)$$

where $\mathbf{U}_{\mathrm{R,s}}$ and $\mathbf{U}_{\mathrm{R,n}}$ are the signal and noise subspaces in this domain, respectively, and $\mathbf{\Sigma}_{\mathrm{R}} = \mathrm{diag}\,(\sigma_{\mathrm{R},1}, \sigma_{\mathrm{R},2}, \ldots, \sigma_{\mathrm{R},N_{\mathrm{R}}})$ is a diagonal matrix, where $\sigma_{\mathrm{R},1}, \ldots, \sigma_{\mathrm{R},N_{\mathrm{R}}}$ are the non-zero singular values of $\mathbf{H}_{(1)}$. The signal subspace matrices in other domain (i.e., $\mathbf{U}_{\mathrm{T,s}}$, $\mathbf{U}_{\mathrm{F,s}}$, and $\mathbf{U}_{\mathrm{TM,s}}$) can be obtained in the same way.

By taking HOSVD of $\mathcal{H}$, the elements of the signal and noise subspaces are separated in all the domains, as shown in Fig. 1, where we combine the receive and transmit antenna space domains (corresponding to the first and second modes of $\mathcal{H}$ in (14)) for illustration. Thus, by constructing the truncated HOSVD model of $\mathcal{H}$ [6], we can suppress the noises in all the domains.

The truncated HOSVD model of $\mathcal{H}$ [6] is given by:

$$\mathcal{H}_{\mathrm{s}} = \mathcal{S}_{\mathrm{s}} \times_1 \mathbf{U}_{\mathrm{R,s}} \times_2 \mathbf{U}_{\mathrm{T,s}} \times_3 \mathbf{U}_{\mathrm{F,s}} \times_4 \mathbf{U}_{\mathrm{TM,s}}, \quad (18)$$

where $\mathcal{S}_{\mathrm{s}} \in \mathbb{C}^{N_{\mathrm{p}} \times N_{\mathrm{p}} \times N_{\mathrm{p}} \times N_{\mathrm{p}}}$ is obtained by discarding the insignificant singular values of $\mathcal{H}$ in all the domains.

By comparing (12) with (18), we have $\mathcal{U}_{\mathrm{s}} \times_4 \mathbf{U}_{\mathrm{TM,s}} = \mathcal{A} \times_4 \mathbf{B}$. Because $\mathbf{U}_{\mathrm{t,s}}$ and $\mathbf{S}$ are full column rank matrices, we obtain

$$\mathcal{A} = \mathcal{U}_{\mathrm{s}} \times_4 \mathbf{D}, \quad (19)$$

where $\mathbf{D} \in \mathbb{C}^{N_{\mathrm{p}} \times N_{\mathrm{p}}}$ is a full rank matrix.

B. PD-based Angle and Delay Estimation

We now use the proposed PD-based algorithm to estimate the angles and delay of each path. We use AOA estimation as an example. For the coupled elevation and azimuth AOAs, we first divide the receive antenna array into three subarrays to decouple them.

We define the AOA baseline selection matrix $\mathbf{J}_{\mathrm{R}} \in \mathbb{R}^{\bar{N}_{\mathrm{R}} \times N_{\mathrm{R}}}$ as

$$[\mathbf{J}_{\mathrm{R}}]_{p_{\mathrm{R}},q_{\mathrm{R}}} = \begin{cases} 1, & \text{if } q_{\mathrm{R}} = p_{\mathrm{R}} + \left\lfloor \frac{p_{\mathrm{R}}-1}{N_{\mathrm{RX}}-1} \right\rfloor, \\ 0, & \text{otherwise,} \end{cases} \tag{20}$$

where $\lfloor \cdot \rfloor$ represents the floor function, $p_{\mathrm{R}} = 1, 2, \ldots, \bar{N}_{\mathrm{R}}$, $q_{\mathrm{R}} = 1, 2, \ldots, N_{\mathrm{R}}$, and $\bar{N}_{\mathrm{R}} = (N_{\mathrm{RX}}-1)(N_{\mathrm{RY}}-1)$.

In (20), when $p_{\mathrm{R}} = m(N_{\mathrm{RX}}-1)+1, \ldots, (m+1)(N_{\mathrm{RX}}-1)$, the floor operator generates

$$\left\lfloor \frac{p_{\mathrm{R}}-1}{N_{\mathrm{RX}}-1} \right\rfloor = m, \ \forall m = 0, 1, \ldots, N_{\mathrm{RY}}-2. \tag{21}$$

Thus, by using (20), for the p_{R}-th row of $\mathbf{J}_{\mathrm{R}}$, only the $(p_{\mathrm{R}} + \lfloor (p_{\mathrm{R}}-1) / (N_{\mathrm{RX}}-1) \rfloor)$-th entry in (20) equals to one, and the other entries are zeros.

We then construct the AOA-related selection matrices as

$$[\mathbf{J}_{\mathrm{R},i}]_{p_{\mathrm{R}},q_{\mathrm{R}}} = \begin{cases} 1, & \text{if } q_{\mathrm{R}} = p_{\mathrm{R}} + \gamma_i + \left\lfloor \frac{p_{\mathrm{R}}-1}{N_{\mathrm{RX}}-1} \right\rfloor, \\ 0, & \text{otherwise,} \end{cases} \tag{22}$$

with $i = 1, 2$. $\gamma_1 = 1$ and $\gamma_2 = N_{\mathrm{RX}}$. Fig. 2 illustrates the subarray division of the receive antenna array. We can see that, by using the proposed selection method, only one antenna element, which is trivial compared to the large number of total antennas, is not selected. Thus, the data collected from almost all of the receive antennas is used for angle estimation.

Based on (19), the AOA baseline subtensor can be formulated as

$$\mathcal{A}_{\mathrm{R}0} = \mathcal{A} \times_1 \mathbf{J}_{\mathrm{R}} = \mathcal{U}_{\mathrm{Rs}} \times_4 \mathbf{D}, \tag{23}$$

where $\mathcal{U}_{\mathrm{Rs}} = \mathcal{U}_{\mathrm{s}} \times_1 \mathbf{J}_{\mathrm{R}}$. Let $\mathcal{A}_{\mathrm{R},i} = \mathcal{A} \times_1 \mathbf{J}_{\mathrm{R},i}$, and then the following linear relations can be obtained:

$$\mathcal{A}_{\mathrm{R},i} = \mathcal{A}_{\mathrm{R}0} \times_4 \mathbf{\Theta}_{\mathrm{R},i}, \tag{24}$$

where

$$[\mathbf{\Theta}_{\mathrm{R},1}]_{l,l} = \exp(j\frac{2\pi d_{\mathrm{R}}}{\lambda_0}\sin(\phi_{\mathrm{R},l})\cos(\theta_{\mathrm{R},l}))$$

and

$$[\mathbf{\Theta}_{\mathrm{R},2}]_{l,l} = \exp(j\frac{2\pi d_{\mathrm{R}}}{\lambda_0}\sin(\phi_{\mathrm{R},l})\sin(\theta_{\mathrm{R},l}))$$

are diagonal matrices. Thus, we can obtain $\mathcal{U}_{\mathrm{R},i} = \mathbf{J}_{\mathrm{R},i}\mathcal{U}_{\mathrm{Rs}} \times_1 \mathbf{J}_{\mathrm{R},i}$, with $i = 1, 2$.

Combining (23) and (24), we can obtain $\mathcal{U}_{\mathrm{R},i} = \mathcal{U}_{\mathrm{Rs}} \times_4 \mathbf{\Psi}_{\mathrm{R},i}$, where $\mathbf{\Psi}_{\mathrm{R},i} = \mathbf{D}\mathbf{\Theta}_{\mathrm{R},i}\mathbf{D}^{-1}$. By using the total least-squares (TLS) criterion, $\mathbf{\Psi}_{\mathrm{R},i}$ can be estimated as $\hat{\mathbf{\Psi}}_{\mathrm{R},i}$. We denote the eigenvalues of $\hat{\mathbf{\Psi}}_{\mathrm{R},i}$ as $\hat{\lambda}_{\mathrm{R},i,l}$. Thus, the azimuth and elevation AOA of the l-th path can be estimated as

$$\hat{\theta}_{\mathrm{R},l} = \arctan\left(\frac{\ln \hat{\lambda}_{\mathrm{R},2,l}}{\ln \hat{\lambda}_{\mathrm{R},1,l}}\right) \tag{25}$$

and

$$\hat{\phi}_{\mathrm{R},l} = \arcsin\left(\frac{\lambda_0}{2\pi d_{\mathrm{R}}}\sqrt{-\left(\ln \hat{\lambda}_{\mathrm{R},1,l}\right)^2 - \left(\ln \hat{\lambda}_{\mathrm{R},2,l}\right)^2}\right), \tag{26}$$

respectively. The azimuth/elevation of AODs can be estimated in the same way.

As for the delay of each path, we define delay-selection matrix as $\mathbf{J}_{\mathrm{F}} = \left[\mathbf{0}_{(N-1)\times 1}, \mathbf{I}_{N-1}\right]$. Then, the delay-related subtensor can be calculated as $\mathcal{A}_{\mathrm{F}} = \mathcal{A} \times_3 \mathbf{J}_{\mathrm{F}}$, and thus the delay of the l-th path can be estimated as

$$\hat{\tau}_l = \frac{1}{N-1}\sum_{\tilde{n}=1}^{N-1}\left[\frac{j\ln(\hat{\lambda}_{\mathrm{F},\tilde{n},l})}{2\pi\Delta_{\mathrm{F}}}\right], \tag{27}$$

where $\hat{\lambda}_{\mathrm{F},\tilde{n},l}$ with $\tilde{n} = 1, 2, \ldots N-1$ are the eigenvalues of estimated $\mathbf{\Psi}_{\mathrm{F}} = \mathbf{D}\mathbf{\Theta}_{\mathrm{F}}\mathbf{D}^{-1}$, and $\mathbf{\Theta}_{\mathrm{F}} = \mathrm{diag}\left(e^{-j2\pi\Delta_{\mathrm{F}}\tau_1}, \ldots, e^{-j2\pi\Delta_{\mathrm{F}}\tau_{N_{\mathrm{p}}}}\right)$.

C. S-PT-based Multiparameter Matching

In the noise-free case, the delay, AOA, and AOD of each path can be matched automatically, because they have the common factor $\mathbf{D}$ in (19). However, in practice, pair matching operation needs to be done due to the presence of noise and estimation error. Traditional pair matching methods need to obtain the approximate values of estimates firstly, and then use exhaustive search (ES) to match all possible pairs of parameters [9]. These methods will lead to extremely high computational complexity if the number of parameters is large.

In [10], a PT-based algorithm was proposed for pair matching. The mismatching is caused by additive noise, which can be mitigated by adding perturbation matrices. Using the azimuth and elevation of AOAs as an example, we have $\mathbf{\Psi}_{\mathrm{R},i} = \mathbf{D}_{\mathrm{R},i}^{-1}\mathbf{\Theta}_{\mathrm{R},i}\mathbf{D}_{\mathrm{R},i}$ and $\mathbf{D}_{\mathrm{R},1} \neq \mathbf{D}_{\mathrm{R},2} \neq \mathbf{D}$ due to the additive noise. By looking for two perturbation matrices $P_{\mathrm{R},1}$ and $P_{\mathrm{R},2}$ such that $\bar{\mathbf{\Psi}}_{\mathrm{R},i} = \mathbf{\Psi}_{\mathrm{R},i} + P_{\mathrm{R},i} = \bar{\mathbf{D}}_{\mathrm{R},i}^{-1}\mathbf{\Theta}_{\mathrm{R},i}\bar{\mathbf{D}}_{\mathrm{R},i}$, we can obtain $\bar{\mathbf{D}}_{\mathrm{R},1} = \bar{\mathbf{D}}_{\mathrm{R},2} = \bar{\mathbf{D}}$ and realize parameter pair matching. The perturbation matrices $P_{\mathrm{R},1}$ and $P_{\mathrm{R},2}$ can be calculated by solving the following problem:

$$\min_{P_{\mathrm{R},1},P_{\mathrm{R},2}} \|P_{\mathrm{R},1}\|_{\mathrm{F}}^2 + \|P_{\mathrm{R},2}\|_{\mathrm{F}}^2 \tag{28}$$

$$s.t. \left(\mathbf{\Psi}_{\mathrm{R},1} + P_{\mathrm{R},1}\right)\left(\mathbf{\Psi}_{\mathrm{R},2} + P_{\mathrm{R},2}\right) = \left(\mathbf{\Psi}_{\mathrm{R},1} + P_{\mathrm{R},2}\right)\left(\mathbf{\Psi}_{\mathrm{R},2} + P_{\mathrm{R},1}\right). \tag{29}$$

The exact solution to this non-linearly constrained problem (28) is in general hard to find, particularly when the parameters we need to pair matching in this paper include delay, azimuth/elevation of AOAs and AODs. It means that there are in total five perturbation matrices we need to calculate. In this paper, we propose an approximate method, S-PT, to realize low-complexity multiparameter pair matching. We assume that the perturbations are small in comparison with $\mathbf{\Psi}_{\mathrm{R},i}$, then the term $P_{\mathrm{R},1}P_{\mathrm{R},2} - P_{\mathrm{R},2}P_{\mathrm{R},1}$ in (29) can be ignored. To further simplify the calculation procedure, we can only add the perturbation to $\mathbf{\Psi}_{\mathrm{R},2}$, i.e., to let $P_{\mathrm{R},1} = 0$. Then $P_{\mathrm{R},2}$ can

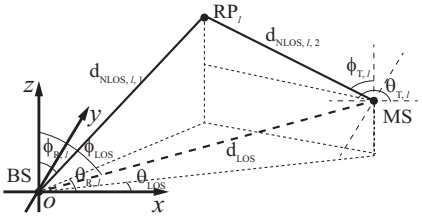

Fig. 3. The geometrical relationship between BS and MS.

be calculated by

$$\begin{aligned}&\text{vec}(P_{\text{R},2})\\&= [\boldsymbol{\Psi}_{\text{R},1}^T \oplus -\boldsymbol{\Psi}_{\text{R},1}]^\dagger \text{vec}(\boldsymbol{\Psi}_{\text{R},1}\boldsymbol{\Psi}_{\text{R},2} - \boldsymbol{\Psi}_{\text{R},2}\boldsymbol{\Psi}_{\text{R},1}),\end{aligned} \tag{30}$$

where $\oplus$ denotes the Kronecker sum. For the five perturbation matrices, that need to be calculated, we can set one of the perturbation matrices to zero, e.g., $P_{\text{F}} = 0$, and use (30) to calculate the rest of them in such a way that automatic pair matching can be achieved.

D. Position Estimation

Once the delay, $\hat{\tau}_l$, and the azimuth/elevation of AOAs and AODs , $\hat{\phi}_{\text{R},l}/\hat{\theta}_{\text{R},l}$ and $\hat{\phi}_{\text{T},l}/\hat{\theta}_{\text{T},l}$, of the l-th path have been obtained by the above mentioned approaches, the location of the MS can be estimated.

In fact, there is a substantially different aspect in terms of signal propagation between mmWave and lower-frequency radio communication systems. The mmWave signal, in practice, will attenuate quickly as it propagates and reflects, and the higher-order bounces (the number of reflections ≥ 2) suffer from high attenuation and can be ignored at the receiver [11]. Therefore, it is reasonable to assume that almost all of the NLOS paths received at BS are from single-bounce reflections. We use the l-th NLOS path, which experiences the reflection from the l-th reflection point (RP_l), to illustrate the process of position estimation. Based on the geometrical relationship between BS and MS, as shown in Fig. 3, we can establish the following equations

$$\begin{cases} d_{\text{LOS}}^2(1-\sin^2\phi_{\text{LOS}}\sin^2\theta_{\text{LOS}}) \\ \quad = d_{l,1}^2(1-\sin^2\hat{\phi}_{\text{R},l}\sin^2\hat{\theta}_{\text{R},l}) \\ \quad +d_{l,2}^2(1-\sin^2\hat{\phi}_{\text{T},l}\sin^2\hat{\theta}_{\text{T},l}) \\ \quad -2d_{l,1}d_{l,2}\cos(\hat{\phi}_{\text{R,XOZ},l}+\hat{\phi}_{\text{T,XOZ},l} \\ \quad \times\sqrt{(1-\sin^2\hat{\phi}_{\text{R},l}\sin^2\hat{\theta}_{\text{R},l})(1-\sin^2\hat{\phi}_{\text{T},l}\sin^2\hat{\theta}_{\text{T},l})} \\ d_{\text{LOS}}^2\sin^2\phi_{\text{LOS}} = d_{l,1}^2\sin^2\hat{\phi}_{\text{R},l}+d_{l,2}^2\sin^2\hat{\phi}_{\text{T},l} \\ \quad -2d_{l,1}d_{l,2}\sin\hat{\phi}_{\text{R},l}\sin\hat{\phi}_{\text{T},l}\cos(\hat{\theta}_{\text{T},l}-\hat{\theta}_{\text{R},l}) \\ d_{\text{LOS}}\sin\phi_{\text{LOS}}\cos\theta_{\text{LOS}} = d_{l,1}\sin\hat{\phi}_{\text{R},l}\cos\hat{\theta}_{\text{R},l} \\ \quad -d_{l,2}\sin\hat{\phi}_{\text{T},l}\cos\hat{\theta}_{\text{T},l} \\ d_{\text{LOS}}\cos\phi_{\text{LOS}} = d_{l,1}\cos\hat{\theta}_{\text{R},l}-d_{l,2}\cos\hat{\theta}_{\text{T},l} \\ d_l = d_{l,1}+d_{l,2} \\ \tan\hat{\phi}_{\text{R,XOZ},l} = \tan\hat{\phi}_{\text{R},l}\cos\hat{\theta}_{\text{R},l} \\ \tan\hat{\phi}_{\text{T,XOZ},l} = -\tan\hat{\phi}_{\text{T},l}\cos\hat{\theta}_{\text{T},l} \end{cases}, \tag{31}$$

where d_{LOS}, θ_{LOS} and ϕ_{LOS} are the length, the azimuth and the elevation of AOA of the virtual LOS path, respectively; $\hat{\phi}_{\text{R,XOZ},l}$ and $\hat{\phi}_{\text{T,XOZ},l}$ are the angles between the positive z-axis and the projections of AOA and AOD of the l-th path on the XOZ plane, respectively; and $d_l = c(\hat{\tau}_l + \tau_{\text{of}})$ is the length of the l-th path, where τ_{of} is the time offset between BS and MS. The l-th path is divided into two parts, whose lengths are denoted as $d_{l,1}$ and $d_{l,2}$, as shown in Fig. 3. Although the time offset, τ_{of}, is unknown, it is a parameter independent of the transmission path. Thus, we can estimate it based on the assumption that two of the estimated NLOS paths converge at a point. By solving (31), the value of d_{LOS}, ϕ_{LOS} and θ_{LOS} can be obtained and denoted as $\hat{d}_{\text{LOS}}$, $\hat{\phi}_{\text{LOS}}$ and $\hat{\theta}_{\text{LOS}}$. Define the position of MS estimated by using the l-th path as $(\hat{x}_l, \hat{y}_l, \hat{z}_l)$. The estimated MS position related to the l-th path can be calculated as

$$\begin{cases} \hat{x}_l = \hat{d}_{\text{LOS}}\sin\hat{\phi}_{\text{LOS}}\cos\hat{\theta}_{\text{LOS}} \\ \hat{y}_l = \hat{d}_{\text{LOS}}\sin\hat{\phi}_{\text{LOS}}\sin\hat{\theta}_{\text{LOS}} \\ \hat{z}_l = \hat{d}_{\text{LOS}}\cos\hat{\phi}_{\text{LOS}} \end{cases}. \tag{32}$$

By using the similar methods to deal with the estimated parameters of all the received paths, we can obtain in total N_{p} solutions, $(\hat{x}_l, \hat{y}_l, \hat{z}_l)$, $l = 0, 1, \ldots, N_{\text{p}}$. Then, the position of MS can be estimated by calculating their mean [1].

V. Simulation Results

In this section, we present simulation results to demonstrate the performance of the proposed algorithm. We set $f_0 = 28$ GHz and $B = 1$ GHz, and assume that there are in total $N_{\text{p}} = 10$ paths and $N = 100$ consecutive subcarriers. The number of transmit antennas along the x- and y-direction is set to $N_{\text{TX}} = N_{\text{TY}} = 10$, and the number of y-directional receive antennas is $N_{\text{RY}} = 10$. The distance, d, between two adjacent antennas is set to $0.5\lambda_0$. We use root mean square error (RMSE) criterion averaged over all the trials to evaluate the performance of the proposed tensor-based positioning method. We also compare it with its reduced version in the matrix form (Here we use "T" for tensor and "M" for matrix to distinguish them), and the extended ESPRIT (E-ESPRIT) [9]. It is noted that due to space limitation, this paper only provides the results for AOA and delay estimations.

Figs. 4(a)-(c) show the RMSE of the estimated azimuth/elevation of AOA and path delay versus the number of receive antennas under different signal-to-noise ratio (SNR) conditions. It can be seen that the RMSE of the estimated parameters decreases as the average received SNR or the number of BS antenna increases. Fig. 4 also shows that the RMSE performance of the proposed tensor-based method outperforms its matrix-based counterpart and E-ESPRIT. This is because that processing the data in the tensor form can suppress more noise components, and our proposed PD-based

[1]It is noted that in practice, diffuse scatterings and higher-order bounces can also be received by BS but their number is much smaller than that of the single bounces. Thus, we can treat all of the received paths as the single-bounce paths and use the proposed method to locate MS, and use clustering algorithms to eliminate the unexpected results before computing the mean.

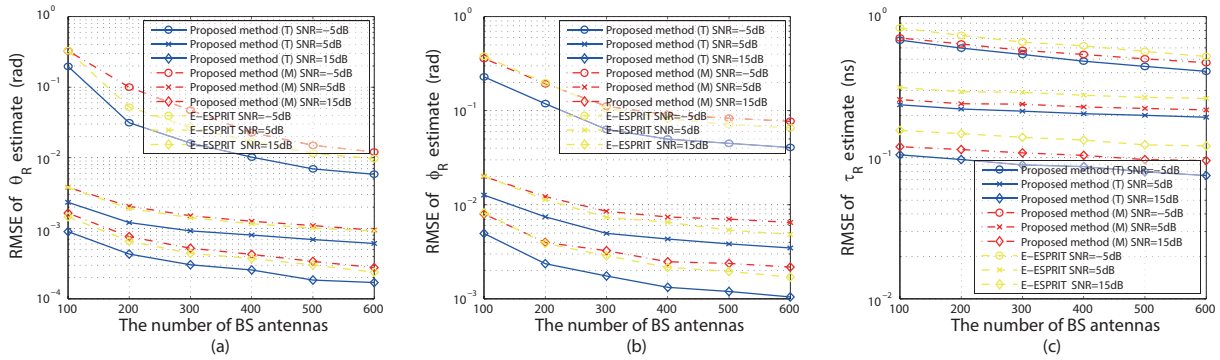

Fig. 4. Comparison of the RMSE performance vs. the number of BS antennas for the estimation of different parameters by the different estimation methods. (a) Azimuth of AOA; (b) Elevation of AOA; (c) Path delay.

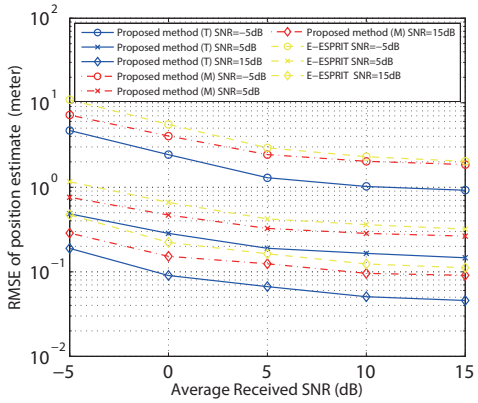

Fig. 5. Comparison of the RMSE performance vs. the number of receive antennas for the MS position estimation.

method (as described in Section IV-B) can use the data collected from almost all of the receive antennas for parameter estimation. We can also observe that the precision of angle estimation of the proposed algorithm in the matrix form is a bit lower than that of E-ESPRIT. This is due to the fact that the preprocessing step, E-MI, is an approximation method and we need to add perturbation matrices in the process of multiparameter matching. However, for delay estimation, our proposed algorithm (whether it is in the tensor form or not) performs better than E-ESPRIT, as shown in Fig. 4(c). This is because by using E-MI-based preprocessing, our algorithm can exploit the high temporal resolution offered by the large bandwidth of mmWave signals.

Fig. 5 shows the RMSE of the estimated target position versus the average received SNR by using different estimation methods. In the simulation, we set the number of receive antennas along the x- and y-direction to $N_{\mathrm{RX}} = N_{\mathrm{RY}} = 20$, and the number of y-directional transmit antennas is fixed at $N_{\mathrm{TY}} = 10$. As shown in Fig. 5, the accuracy of the positioning estimation increases with the increase of the average received SNR. It also shows that although the angle estimation precision of our matrix-form method is slightly lower than that of E-ESPRIT, due to the superiority in delay estimation, it outperforms E-ESPRIT in terms of localization performance.

VI. CONCLUSIONS

We have now presented a novel 3D NLOS positioning method for wideband mmWave massive MIMO systems. An E-MI-based method is designed firstly, and a PD-based tensor multiparameter estimation algorithm is then proposed to process the high-dimensional data and realize precise 3D target localization in the presence of multiple propagation paths. In order to reduce the computational complexity, an S-PT-based method is proposed for multiparameter matching. Simulation results show that the proposed method can achieve improved performance in 3D localization.

REFERENCES

[1] A. Guerra, F. Guidi, and D. Dardari, "Position and orientation error bound for wideband massive antenna arrays," in *Proc. IEEE Int. Conf. on Commun. Workshops (ICCW)*, London, UK, Jun. 2015, pp. 1–6.

[2] Z. Lin, T. Lv, and P. T. Mathiopoulos, "3-D indoor positioning for millimeter-Wave massive MIMO systems," *IEEE Trans. Commun.*, vol. 66, no. 6, pp. 2472–2486, June 2018.

[3] M. Vari and D. Cassioli, "mmWaves RSSI indoor network localization," in *Proc. IEEE Int. Conf. on Commun. Workshop (ICCW)*, Sydney, Australia, Jun. 2014, pp. 127–132.

[4] F. Roemer, M. Haardt, and G. Del Galdo, "Analytical performance assessment of multi-dimensional matrix- and tensor-based ESPRIT-type algorithms," *IEEE Trans. Signal Process.*, vol. 62, no. 10, pp. 2611–2625, May 2014.

[5] B. D. Van Veen and K. M. Buckley, "Beamforming: A versatile approach to spatial filtering," *IEEE Acoust. Speech Sig. Proc. Mag.*, vol. 5, no. 5, pp. 4–24, Apr. 1988.

[6] Lieven De Lathauwer, Bart De Moor, and Joos Vandewalle, "A multilinear singular value decomposition," *SIAM J. Matrix Anal. Appl.*, vol. 21, no. 4, pp. 1253–1278, Mar. 2000.

[7] F. Raimondi, P. Comon, and O. Michel, "Wideband multilinear array processing through tensor decomposition," in *Proc. IEEE Int. Conf. Acoust. Speech Signal Process. (ICASSP)*, Shanghai, China, Mar. 2016, pp. 2951–2955.

[8] C. E. Shannon, "Communication in the presence of noise," *Proceedings of the IRE*, vol. 37, no. 1, pp. 10–21, Jan. 1949.

[9] A. Hu, T. Lv, H. Gao, Z. Zhang, and S. Yang, "An ESPRIT-based approach for 2-D localization of incoherently distributed sources in massive MIMO systems," *IEEE J. Sel. Topics Signal Process.*, vol. 8, no. 5, pp. 996–1011, Oct. 2014.

[10] A. J. van der Veen, P.B. Ober, and E.F. Deprettere, "Azimuth and elevation computation in high resolution doa estimation," *IEEE Trans. Signal Process.*, vol. 40, no. 7, pp. 1828–1832, July 1992.

[11] T. S. Rappaport, E. Ben-Dor, J. N. Murdock, and Y. Qiao, "38 GHz and 60 GHz angle-dependent propagation for cellular & peer-to-peer wireless communications," in *IEEE Intl. Conf. on Comm. (ICC)*, Ottawa, Canada, Jun. 2012, pp. 4568–4573.